


Reynolds scaling analysis of the Landau–de Gennes equations for nematic liquid crystals

Shancheng Li, Somesh Bhatia , and Dana Grecov*

Department of Mechanical Engineering, University of British Columbia, 2054–6250 Applied Science Lane, Vancouver, Canada, BC V6T 1Z4

 (Received 15 March 2022; accepted 15 November 2022; published 28 December 2022)

The liquid crystal (LC) is a state of matter that is intermediate between crystalline solid and amorphous liquid. They are anisotropic viscoelastic materials with broad applications in science and engineering, including as lubricants or additives to lubricants to reduce wear, improve load-carrying capacity, and decrease the coefficient of friction. In this paper, the Landau–de Gennes (LdG) equations are used to model the flow of LCs. The LdG equations are simplified using the Reynolds scaling analysis to form the simplified LdG equations, which are then applied to a Couette geometry and a slider bearing geometry. Both the simplified LdG model and the full LdG model are numerically solved in COMSOL Multiphysics®. The simplified LdG model is evaluated and verified by comparing the simulation results of the simplified LdG model with those from the full LdG model. Lubrication performance is analyzed for the slider bearing geometry with both the simplified LdG model and the full LdG model. The simplified LdG model significantly reduces simulation wall time compared to the full LdG model over the same domains.

DOI: [10.1103/PhysRevFluids.7.123303](https://doi.org/10.1103/PhysRevFluids.7.123303)

I. INTRODUCTION

Liquid crystals (LCs) are defined as a state of matter that is intermediate between crystalline solid and amorphous liquid [1]. LCs have a variety of applications leading to much industrial and academic research to understand their behavior to characterize their physical properties. In particular, due to their ability to form ordered layers close to the boundaries, LCs are used as lubricants to reduce wear and decrease the losses of energy caused by friction; there is an increasing interest in studying the lubrication that occurs in the joints of the human body with LCs as lubricants [2–9].

There are a variety of theories that can model the flow of LCs. The continuum-based vectorial Ericksen-Leslie (EL) theory and the mesoscopic tensorial Landau–de Gennes (LdG) theory are such examples. In the LdG theory, the microstructure of the nematic LCs can be described based on a second-order, symmetric, and traceless tensor order parameter \mathbf{Q} [10]. The LdG theory is a complete and well-established theory that considers both short-range order elasticity due to the intermolecular forces and long-range order elasticity due to the surface effects. Therefore, the LdG equations coupled with the Navier-Stokes equations with a modified stress tensor to account for the anisotropic and viscoelastic contributions can model fast flows and short length scale phenomena such as defect nucleation, which the continuum-based EL theory fails to achieve [11–13]. The LdG theory has been applied to simulate simple shear flow, the flow in eccentric cylinders of nematic LCs, as well as a three-dimensional (3D) flow in the geometry of a hip joint [5,9,14–16]. In addition to the LdG theory, other models have been used to describe the flow of LCs. In the Beris-Edwards model

*Corresponding author: dgrecov@mech.ubc.ca

[17], the Poisson bracket formulation is used to obtain the governing equations. The Qian-Sheng model [18] is also used to describe the hydrodynamics of LC flows.

Although the LdG theory is a well-established and complete theory, it is highly complex, thus making solving the full LdG equations numerically time consuming and involving large amounts of memory. The LdG equations can be simplified in thin-gap geometries by the Reynolds scaling analysis, also known as lubrication theory. The simplified LdG model can significantly reduce simulation time, thus reducing the computational resource required. Since its introduction by Osborne Reynolds in 1886 [19], lubrication theory has been widely applied in the study of various flows [20]. The fundamental assumption of lubrication theory is that the distance between two boundaries is much smaller than the lateral gap width [20], which allows the use of order analysis to eliminate insignificant derivative terms in the governing equation. Lubrication theory can be applied to thin gaps where the two boundaries of the flow are not parallel, in which the 1D flow assumption cannot be used because the primary velocity component must be a function of the distance in the flow direction [20]. Although lubrication theory was originally applied to flows of Newtonian fluids, it has been extended to other fluids and flows such as the flows of non-Newtonian fluids and flows in special geometries. Tichy [21] developed the hydrodynamic lubrication theory for the Bingham plastic flow model as a non-Newtonian fluid and applied the model to the squeeze film damper and the journal bearing to predict bearing behavior. He also simplified the EL theory using the Reynolds scaling analysis for the LC flow in a slider bearing geometry [22]. Constantinescu [23] developed a model for the hydrodynamic turbulent motion in the lubricant layer by using the Prandtl mixing length hypothesis. Naduvinamani and Marali [24] derived a generally modified Reynolds-type equation of porous sliding-squeezing surfaces to assess the characteristics of bearings with such structures. Roberts *et al.* [25] developed an extension of Reynolds lubrication theory to model the effect of free fluid interfaces and FSI in lubrication films, implemented in a general 3D FEA code. Takeuchi and Gu [26] proposed an extended lubrication model by taking into consideration a larger surface-to-surface distance compared with that for the Reynolds lubrication theory. Amar and Cummings [27] investigated the fingering instabilities in thin nematic films by applying lubrication theory to the EL theory describing the free boundary evolution of a thin nematic film. Applying lubrication theory to the EL theory, Cummings [28] later derived a model describing the evolution of the film height under gravity for nematic LCs.

The flow in bearing geometries has been investigated and studied extensively [29–34,16]. Ballal and Rivlin [29] established a model describing the flow of a Newtonian fluid between two eccentric rotating cylinders. Using the Phan-Thien-Tanner constitutive equations to model thin-film flows, Li [30] investigated whether viscoelasticity had an effect on lubrication performance in thin-film flows and found that viscoelasticity increased the lubricant pressure field and had an advantageous effect on lubrication performance. Grecov and Clermont [31] investigated non-Newtonian flows between eccentric cylinders by means of the stream-tube method and domain decomposition and found that viscoelasticity increased load, stress, and torque when compared to Newtonian flows. Noroozi and Grecov [16] solved the transient flow of nematic LCs between two eccentric cylinders numerically with the LdG theory and showed that the flow with LCs has significantly larger pressure, first normal stress difference, and wall shear stress compared to Newtonian cases. In [32], Dorier and Tichy studied the behavior of a Bingham-like viscous fluids in several lubrication flows by presenting a generalized Reynolds equation, which was later applied to a plane slider bearing and to two parallel plates. Buckholz [33] investigated the effects of power-law, non-Newtonian lubricants on load capacity and friction for plane slider bearings by utilizing a modified Reynolds equation. Chu, Hsu, and Chen [34] proposed an analytical approach for the analysis of slider bearings with non-Newtonian lubricants and subsequently computed various lubrication properties, such as the load capacity and the friction coefficient. The flow in slider bearing geometries plays an important role in the understanding of lubrication behavior in synovial joints. In their research, Kupchinov *et al.* [35] confirmed the existence of liquid crystalline cholesterol compounds in human and animal synovial fluids extracted 12 h postmortem. Their tribological experiments indicated that the presence of such compounds resulted in low friction of the synovial joints. Bujurke [36]

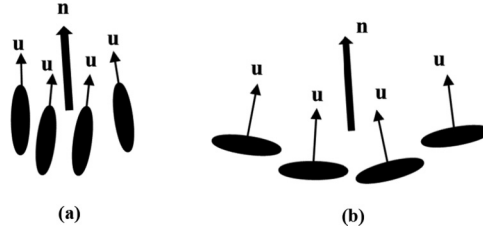


FIG. 1. Schematic representation of director \mathbf{n} for (a) Calamitic, and (b) Discotic LCs.

investigated the lubrication behavior of a fluid with reference to synovial joints in slider bearings and found that a normal young synovial fluid sample had significantly higher load capacity, friction force, and coefficient friction than old and osteoarthritic synovial fluid samples. Very few studies investigated the flow of LCs in slider bearing geometries. Tichy [22] simplified the EL theory using the Reynolds scaling analysis for the LC flow in a slider bearing geometry and found that microstructural orientation, the couple viscosity parameter, and material properties could affect lubrication properties. In addition, because of the EL theory's limited applicability in sufficiently slow flows [37], it is of interest to apply the Reynolds scaling analysis to the LdG theory, which has broader validity than the EL theory.

One objective of this study is to simplify the LdG model using the Reynolds scaling analysis (lubrication theory) and to apply the simplified LdG equations to different geometries: the flow of LCs between parallel plates and the flow in a slider bearing geometry. Another objective is to evaluate the lubrication performance of the slider bearing. The application of the simplified LdG equations to the flow between parallel plates primarily serves to evaluate and verify the simplified LdG model. The organization of this article is as follows: First, we present the full LdG model for the flow of LC crystals, followed by the lubrication approximation of the LdG model, namely the simplified LdG model, as well as the simplified momentum equations. Then, selected results from the full LdG model and the simplified LdG model applied to the two lubrication geometries are presented for the evaluation and verification of the simplified LdG model as well as for the computation of lubrication properties. Finally, we present some conclusions.

II. THEORY AND GOVERNING EQUATIONS

The microstructure of the nematic LCs can be described based on the second-order, symmetric, and traceless tensor order parameter \mathbf{Q} [10], as defined below:

$$\mathbf{Q} = \int \left(\mathbf{u}\mathbf{u} - \frac{1}{3}\mathbf{I} \right) \omega d^2\mathbf{u}. \quad (1)$$

Here \mathbf{u} is the unit vector showing the orientation of molecules of the nematic, as shown in Fig. 1, \mathbf{I} represents the unit tensor, and ω is the orientation distribution function. Alternatively, \mathbf{Q} can be represented based on the eigenvectors (\mathbf{n} , \mathbf{m} , \mathbf{l}) and eigenvalues (λ_n , λ_m , λ_l) as shown in Eq. (2):

$$\mathbf{Q} = \lambda_n \mathbf{n}\mathbf{n} + \lambda_m \mathbf{m}\mathbf{m} + \lambda_l \mathbf{l}\mathbf{l}. \quad (2)$$

The eigenvalues can be defined as functions of the scalar order parameter S and the biaxial order parameter P [12] as shown in Eq. (3):

$$\lambda_n = \frac{2}{3}S; \quad \lambda_m = -\frac{1}{3}(S - P); \quad \lambda_l = -\frac{1}{3}(S + P). \quad (3)$$

The scalar order parameter S measures the molecular alignment along with the director \mathbf{n} . In LCs, S usually ranges between 0 and 1 with 1 corresponding to perfect orientational order and 0 absolute randomness.

The LdG theory is a tensorial theory and the \mathbf{Q} tensor described earlier is used to describe the orientation variable. The governing equation of the theory follows from the dissipation function Δ [14]:

$$\Delta = \boldsymbol{\tau}_s : \mathbf{A} + cKT\mathbf{H} \cdot \hat{\mathbf{Q}}. \quad (4)$$

Here, $\boldsymbol{\tau}_s$ is the symmetric viscoelastic stress tensor, c represents the concentration of molecules in the liquid crystalline state, K is the Boltzmann constant, and T is the absolute temperature. \mathbf{A} is the rate-of-strain tensor, \mathbf{H} is the molecular field, and $\hat{\mathbf{Q}}$ is the Jaumann derivative of the order parameter tensor. The tensors are as follows:

$$\mathbf{A} = \frac{1}{2}(\nabla\mathbf{u} + \nabla\mathbf{u}^T), \quad (5)$$

$$\hat{\mathbf{Q}} = \frac{\partial\mathbf{Q}}{\partial t} + (\mathbf{u} \cdot \nabla)\mathbf{Q} - \mathbf{W} \cdot \mathbf{Q} + \mathbf{Q} \cdot \mathbf{W}, \quad (6)$$

$$cKT\mathbf{H} = -\left[\frac{\delta F}{\delta\mathbf{Q}}\right]^{[s]} = \left[\frac{\partial f}{\partial\mathbf{Q}} - \nabla \cdot \left(\frac{\partial f}{\partial\nabla\mathbf{Q}}\right)\right]^{[s]}. \quad (7)$$

Here, \mathbf{W} is the vorticity tensor, \mathbf{u} is the velocity vector, F is the total free energy, and f is the free energy density. \mathbf{W} and f are defined as

$$\mathbf{W} = \frac{1}{2}(\nabla\mathbf{u} - \nabla\mathbf{u}^T), \quad (8)$$

$$f = (cKT) \left[\frac{1}{2} \left(1 - \frac{\mathfrak{A}}{3}\right) (\mathbf{Q} : \mathbf{Q}) - \frac{1}{3} \mathfrak{A} [\mathbf{Q} : (\mathbf{Q} \cdot \mathbf{Q})] + \frac{1}{4} \mathfrak{A} (\mathbf{Q} : \mathbf{Q})^2 \right. \\ \left. + \frac{L_1}{2cKT} \{\nabla\mathbf{Q} : (\nabla\mathbf{Q})^T\} + \frac{L_2}{2cKT} (\nabla \cdot \mathbf{Q}) \cdot (\nabla \cdot \mathbf{Q}) \right]. \quad (9)$$

Here $\mathfrak{A} = 3T^*/T$ is the nematic potential where T^* is the isotropic-nematic transition temperature, L_i refers to the Landau coefficients, and the superscript $[s]$ means symmetric and traceless [14]. The molecular field \mathbf{H} can be calculated as

$$(cKT)\mathbf{H} = (cKT) \left[\frac{(\frac{\mathfrak{A}}{3} - 1)\mathbf{Q} + \mathfrak{A}\mathbf{Q} \cdot \mathbf{Q} - \mathfrak{A}(\mathbf{Q} : \mathbf{Q}) \cdot (\mathbf{Q} + \frac{1}{3}\mathbf{I})}{2} \right. \\ \left. + \frac{L_1}{cKT} \nabla^2\mathbf{Q} + \frac{L_2}{2cKT} \{\nabla(\nabla \cdot \mathbf{Q}) + [\nabla(\nabla \cdot \mathbf{Q})]^T - \frac{2}{3}[\text{tr}\nabla(\nabla \cdot \mathbf{Q})]\mathbf{I}\} \right]. \quad (10)$$

The above expression contains both short-range and long-range contributions. The dynamics of the tensor order parameter are given by

$$\hat{\mathbf{Q}} = \mathbf{F}(\nabla\mathbf{u}, \mathbf{Q}) + \mathbf{H}^{\text{sr}}(\overline{D}_r, \mathbf{Q}) + \mathbf{H}^{\text{lr}}(\overline{D}_r, \nabla\mathbf{Q}). \quad (11)$$

Here, \mathbf{F} represents the flow contribution, \mathbf{H}^{sr} represents the short-range contribution, and \mathbf{H}^{lr} represents the long-range contribution [15]. Their expressions are

$$\mathbf{F} = \frac{2}{3}\beta\mathbf{A} + \beta \left[\mathbf{A} \cdot \mathbf{Q} + \mathbf{Q} \cdot \mathbf{A} - \frac{2}{3}(\mathbf{A} : \mathbf{Q})\mathbf{I} \right] \\ - \frac{1}{2}\beta(\mathbf{A} : \mathbf{Q})\mathbf{Q} + \mathbf{A} \cdot \mathbf{Q} \cdot \mathbf{Q} + \mathbf{Q} \cdot \mathbf{A} \cdot \mathbf{Q} + \mathbf{Q} \cdot \mathbf{Q} \cdot \mathbf{A} - [(\mathbf{Q} \cdot \mathbf{Q}) : \mathbf{A}]\mathbf{I}, \quad (12)$$

$$\mathbf{H}^{\text{sr}} = 6\overline{D}_r \left[\left(\frac{\mathfrak{A}}{3} - 1\right)\mathbf{Q} + \mathfrak{A}\mathbf{Q} \cdot \mathbf{Q} - \mathfrak{A}(\mathbf{Q} : \mathbf{Q}) \cdot \left(\mathbf{Q} + \frac{1}{3}\mathbf{I}\right) \right], \quad (13)$$

$$\mathbf{H}^{\text{lr}} = \frac{L_1}{cKT} \nabla^2\mathbf{Q} + \frac{L_2}{2cKT} \left\{ \nabla(\nabla \cdot \mathbf{Q}) + [\nabla(\nabla \cdot \mathbf{Q})]^T - \frac{2}{3}[\text{tr}\nabla(\nabla \cdot \mathbf{Q})]\mathbf{I} \right\}. \quad (14)$$

Here, β is a thermodynamic parameter [14] and \overline{D}_r is the microstructural rotational diffusivity which is defined as [14]

$$\overline{D}_r(\mathbf{Q}) = D_r \left[1 - \frac{3}{2}(\mathbf{Q} : \mathbf{Q})\right]^{-2}. \quad (15)$$

Here, D_r is the preaveraged rotational diffusivity. It is to be noted that taking $\overline{D_r}$ independent of \mathbf{Q} results in spurious results for nematic LCs as the tumbling and wagging regimes are not predicted [12].

The equilibrium value of the scalar order parameter S_{eq} can be calculated as shown [15] below:

$$S_{\text{eq}} = 0.25 + 0.75\sqrt{1 - \frac{8}{3\Omega}}. \quad (16)$$

Due to the existence of LC molecules, the stress tensor of the Navier-Stokes equations must be modified to account for the properties of LCs. The total stress tensor $\boldsymbol{\sigma}$ is defined as the sum of three main components: the symmetric component $\boldsymbol{\tau}_s$, the asymmetric component $\boldsymbol{\tau}_a$, and the Ericksen stress tensor $\boldsymbol{\tau}_{\text{Er}}$. The symmetric stress component is the sum of the viscous term and the elastic term, $\boldsymbol{\tau}_s = \boldsymbol{\tau}_v + \boldsymbol{\tau}_e$. Therefore

$$\boldsymbol{\sigma} = \boldsymbol{\tau}_v + \boldsymbol{\tau}_e + \boldsymbol{\tau}_a + \boldsymbol{\tau}_{\text{Er}}. \quad (17)$$

Individual terms of the stress tensor are

$$\begin{aligned} \boldsymbol{\tau}_v = & v_1 \mathbf{A} + v_2 [\mathbf{Q} \cdot \mathbf{A} + \mathbf{A} \cdot \mathbf{Q} - \frac{2}{3}(\mathbf{Q} : \mathbf{A})\mathbf{I}] \\ & + v_4 (\mathbf{A} : \mathbf{Q})\mathbf{Q} + \mathbf{A} \cdot \mathbf{Q} \cdot \mathbf{Q} + \mathbf{Q} \cdot \mathbf{A} \cdot \mathbf{Q} + \mathbf{Q} \cdot \mathbf{Q} \cdot \mathbf{A} + [(\mathbf{Q} : \mathbf{Q})\mathbf{A}]\mathbf{I}, \end{aligned} \quad (18)$$

$$\begin{aligned} \boldsymbol{\tau}_e = & cKT \left\{ -\frac{2\beta}{3}\mathbf{H} - \beta \left[\mathbf{H} \cdot \mathbf{Q} + \mathbf{Q} \cdot \mathbf{H} - \frac{2}{3}(\mathbf{H} : \mathbf{Q})\mathbf{I} \right] \right. \\ & \left. + \frac{\beta}{2} \{ (\mathbf{H} : \mathbf{Q})\mathbf{Q} + \mathbf{H} \cdot \mathbf{Q} \cdot \mathbf{Q} + \mathbf{Q} \cdot \mathbf{H} \cdot \mathbf{Q} + \mathbf{Q} \cdot \mathbf{Q} \cdot \mathbf{H} + [(\mathbf{Q} : \mathbf{Q})\mathbf{I}] \} \right\}, \end{aligned} \quad (19)$$

$$\boldsymbol{\tau}_a = cKT \{ \mathbf{H} \cdot \mathbf{Q} - \mathbf{Q} \cdot \mathbf{H} \}, \quad (20)$$

$$\boldsymbol{\tau}_{\text{Er}} = L_1 \{ L^* (\nabla \cdot \mathbf{Q}) \cdot (\nabla \mathbf{Q})^T - \nabla \mathbf{Q} : (\nabla \mathbf{Q})^T \}, \quad (21)$$

where $\mathbf{H} = \mathbf{H}^{\text{sr}} + \mathbf{H}^{\text{lr}}$ is the sum of short-range and long-range elasticities, v_i 's are the Landau viscosity coefficients, and $L^* = L_2/L_1$ is the dimensionless Landau coefficient [14,15]. Therefore, the incompressible continuity equation and the dimensional momentum equations with no gravity and other external fields are shown below:

$$\nabla \cdot \mathbf{u} = 0, \quad (22)$$

$$\rho \frac{D\mathbf{u}}{Dt} = -\nabla p + \nabla \cdot \boldsymbol{\sigma}, \quad (23)$$

where ρ is a characteristic density, t is the time, and p is the pressure.

A. Nondimensional full LdG equations

The nondimensional equations of the full theory have been presented multiple times previously [9,14–16] and so the derivation is not included in this work. However, since the equations are numerically solved, they are shown below for the sake of completeness. Considering the flow to have a velocity scale U and a length scale L the nondimensional form is as shown in Eqs. (24)–(29).

The evolution equation is

$$\hat{\mathbf{Q}} = \mathbf{F} + \left(\frac{1}{\text{De}} \right) \mathbf{H}^{\text{sr}} + \left(\frac{1}{\text{Er}} \right) \mathbf{H}^{\text{lr}}. \quad (24)$$

In Eq. (24), the following nondimensional numbers are selected:

Ericksen number: $\text{Er} = \frac{U H c K T}{6 L_1 D_r}$; Deborah number: $\text{De} = \frac{U}{6 H D_r}$; energy ratio: $\text{R} = \frac{\text{Er}}{\text{De}}$;

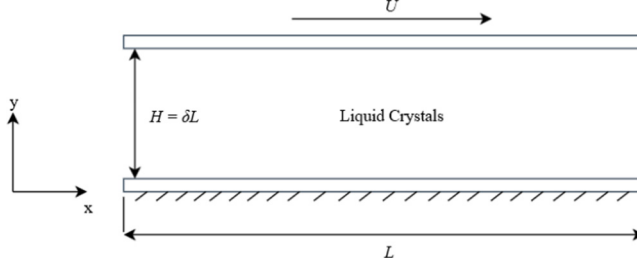


FIG. 2. Couette flow geometry.

Reynolds number: $Re = \frac{\rho U^2}{cKT}$, where H is a characteristic length scale and U is a characteristic velocity scale.

Due to its complexity, the LC flow has multiple time scales and length scales [38,39]. The time scales and length scales with their corresponding symbols are shown below [38,39]: external length scale l_e ; flow length scale l_f ; internal length scale l_i ; external time scale τ_e ; flow time scale τ_f ; internal time scale τ_i .

Their expressions are

$$l_e = H, \quad l_f = \sqrt{\frac{2L_1 D_r}{cKT \dot{\gamma}}}, \quad l_i = \sqrt{\frac{L_1}{3cKT}}, \quad l_i \ll l_e, \quad (25)$$

$$\tau_e = \frac{cKTL^2}{2D_r L_1}, \quad \tau_f = \frac{1}{\dot{\gamma}}, \quad \tau_i = \frac{1}{D_r}, \quad \tau_i \ll \tau_e, \quad (26)$$

where $\dot{\gamma} = \frac{U}{H}$ is the shear rate.

The momentum equations are shown in Eq. (27) with the asterisk used for dimensionless variables,

$$Re \left\{ \frac{\partial \mathbf{u}^*}{\partial t^*} + (\mathbf{u}^* \cdot \nabla) \mathbf{u}^* \right\} = -\nabla p^* + De(\nabla \cdot \boldsymbol{\tau}_v^*) + (\nabla \cdot \boldsymbol{\tau}_e^*) + (\nabla \cdot \boldsymbol{\tau}_a^*) + \frac{1}{R}(\nabla \cdot \boldsymbol{\tau}_{Er}^*). \quad (27)$$

The dimensionless total stress tensor takes the form shown as follows:

$$\boldsymbol{\sigma}^* = \boldsymbol{\tau}_a^* + \boldsymbol{\tau}_e^* + \left(\frac{Er}{R} \right) \boldsymbol{\tau}_v^* + \left(\frac{1}{R} \right) \boldsymbol{\tau}_{Er}^*. \quad (28)$$

In Eq. (28), the total stress tensor is nondimensionalized using

$$\boldsymbol{\sigma}^* = \boldsymbol{\sigma}/cKT, \quad v_1^* = (v_1 6D_r)/(cKT), \quad v_2^* = (v_2 6D_r)/(cKT), \quad v_4^* = (v_4 6D_r)/(cKT), \quad (29)$$

where v_1^* , v_2^* , and v_4^* are the dimensionless Landau viscosity coefficients.

B. Nondimensional simplified LdG equations

This section consists of the major assumptions for the simplification of the full LdG equations with the scaling analysis and the resulting simplified LdG equations. Figure 2 is the flow geometry used in the simplification process. It shows a typical Couette flow geometry with the upper plate moving to the right and the lower plate staying stationary.

As shown in Fig. 2, the length scale along the x direction is assumed to be L and the length scale along the y direction is $H = \delta L$ with $\delta \ll 1$. The driving velocity U is selected as the velocity scale for the u velocity.

The incompressible continuity equation is first nondimensionalized to obtain the velocity scale for the v velocity V . Given the scales, it is clear that

$$u^* = \frac{u}{U}, \quad v^* = \frac{v}{V}, \quad (30)$$

where the asterisk indicates dimensionless variables. To balance the scales in the continuity equation, it is clear that

$$V = \delta U. \quad (31)$$

Following the procedure in [14], to nondimensionalize the evolution equations of the \mathbf{Q} tensor, the following variables are nondimensionalized as follows:

$$t^* = \dot{\gamma} t, \quad \mathbf{A}^* = \frac{\mathbf{A}}{\dot{\gamma}}, \quad \mathbf{W}^* = \frac{\mathbf{W}}{\dot{\gamma}}, \quad \nabla^* = L \nabla, \quad (32)$$

where $\dot{\gamma} = \frac{U}{L}$, as the shear rate, is used to scale the time t . The velocity gradients in the shear rate tensor \mathbf{A} and the vorticity tensor \mathbf{W} are nondimensionalized one by one. For instance,

$$A_{12}^* = \frac{1}{2} \left(\frac{U}{\delta L} \frac{\partial u^*}{\partial y^*} + \frac{\delta U}{L} \frac{\partial v^*}{\partial x^*} \right). \quad (33)$$

Since it is assumed that $\delta \ll 1$, $\frac{U}{\delta L} \frac{\partial u^*}{\partial y^*}$ is the dominant term and the second term is dropped. Therefore

$$A_{12}^* = \frac{1}{2} \left(\frac{U}{\delta L} \frac{\partial u^*}{\partial y^*} \right). \quad (34)$$

All terms in the evolution equations are nondimensionalized in this manner and only terms of $O(\frac{1}{\delta})$ remain as δ is considered far smaller than 1. As in other lubrication analyses, the evolution equation is assumed to be steady.

In this research, the strong planar anchoring condition is assumed at the boundary and the director \mathbf{n} is assumed to remain in the xy plane; therefore the tensor order parameter \mathbf{Q} has only three independent components: Q_{11} , Q_{12} , and Q_{22} [37]. Thus, the resultant nondimensionalized evolution equations (the simplified LdG equations) with the asterisk dropped are

$$\begin{aligned} & \left(\frac{1}{\text{Er}} \right) \left(\frac{\partial^2}{\partial y^2} (Q_{11}) - \frac{L^*}{3} \frac{\partial^2}{\partial y^2} (Q_{22}) \right) \\ & + \left(\frac{1}{\text{De}} \right) \left(-\mathfrak{A} (Q_{11}^2 + 2Q_{12}^2 + Q_{22}^2 + (Q_{11} + Q_{22})^2) (Q_{11} + \frac{1}{3}) \right) \\ & = -\frac{\partial u}{\partial y} [1 - 3(Q_{11}^2 + Q_{12}^2 + Q_{22}^2 + Q_{11}Q_{22})]^2 \left[Q_{12} \left(1 + \frac{\beta}{3} \right) - \beta Q_{11}Q_{12} \right], \quad (35) \\ & \left(\frac{1}{\text{Er}} \right) \left[\left(1 + \frac{L^*}{2} \right) \frac{\partial^2}{\partial y^2} (Q_{12}) \right] + \left(\frac{1}{\text{De}} \right) \left(-\mathfrak{A} Q_{12} (Q_{11}^2 + 2Q_{12}^2 + Q_{22}^2 + (Q_{11} + Q_{22})^2) \right) \\ & = \frac{\partial u}{\partial y} [1 - 3(Q_{11}^2 + Q_{12}^2 + Q_{22}^2 + Q_{11}Q_{22})]^2 \\ & \times \left[Q_{11} \left(\frac{1-\beta}{2} \right) - Q_{22} \left(\frac{\beta+1}{2} \right) + \frac{\beta}{4} Q_{11}^2 + \frac{5\beta}{4} Q_{12}^2 + \frac{\beta}{4} Q_{22}^2 - \frac{\beta}{3} + \frac{\beta}{4} Q_{11}Q_{22} \right], \quad (36) \end{aligned}$$

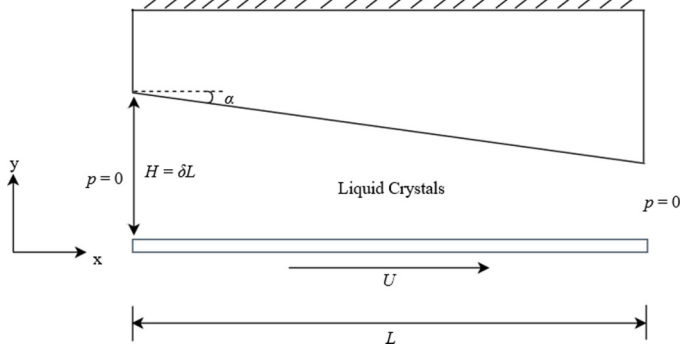


FIG. 3. Slider bearing geometry.

$$\begin{aligned} & \left(\frac{1}{\text{Er}}\right) \left[\left(1 + \frac{2L^*}{3}\right) \frac{\partial^2}{\partial y^2} (Q_{22}) \right] + \left(\frac{1}{\text{De}}\right) \left(-\mathfrak{A} (Q_{11}^2 + 2Q_{12}^2 + Q_{22}^2 + (Q_{11} + Q_{22})^2) (Q_{22} + \frac{1}{3}) \right) \\ & = \frac{\partial u}{\partial y} \left[1 - 3(Q_{11}^2 + Q_{12}^2 + Q_{22}^2 + Q_{11}Q_{22}) \right]^2 \left[Q_{12} \left(1 - \frac{\beta}{3}\right) + \beta Q_{12}Q_{22} \right], \end{aligned} \quad (37)$$

where $\text{Er} = \frac{U\delta LcKT}{6L_1D_r}$, $\text{De} = \frac{U}{6\delta LD_r}$, and $R = \frac{\text{Er}}{\text{De}}$. Note that the definitions of Er, De, and R are consistent with the previous definitions in Eq. (24) with the length scale H replaced by δL , the gap size.

To nondimensionalize the momentum equations, the total stress tensor is nondimensionalized similarly to Eq. (29):

$$\boldsymbol{\sigma}^* = \boldsymbol{\sigma}/(cKT). \quad (38)$$

To nondimensionalize the stress terms in the momentum equations, it is assumed that the y derivative is much greater than the x derivative so that all x derivatives are neglected.

The pressure term is scaled as follows:

$$p^* = \frac{p}{P_0}, \quad (39)$$

where P_0 is a pressure scale, selected as $P_0 = \frac{cKT}{\delta}$ [20,40,41]. Then, assuming the momentum equations are steady, and dropping negligible terms, the final simplified dimensionless momentum equations with the asterisk dropped are

$$\left(-\frac{\partial p}{\partial x}\right) + \text{De} \frac{\partial \tau_{12}^v}{\partial y} + \frac{\partial \tau_{12}^E}{\partial y} + \frac{\partial \tau_{12}^a}{\partial y} + \frac{1}{R} \frac{\partial \tau_{12}^{\text{Er}}}{\partial y} = 0, \quad (40)$$

$$\left(-\frac{\partial p}{\partial y}\right) = 0. \quad (41)$$

III. METHODOLOGY

The simplified LdG equations are evaluated and verified by comparing the simulation results with those from the full LdG equations. Both sets of equations are solved in COMSOL Multiphysics® 5.6 for both the Couette flow geometry and the slider bearing geometry, as shown in Figs. 2 and 3. In the slider bearing geometry, due to the existence of the pitch angle α , the pressure gradient is no longer zero, which allows the evaluation of lubrication performance. Figure 3 shows a typical slider bearing geometry with a stationary upper plate and a moving lower plate.

In order to evaluate and verify the solutions obtained from lubrication theory, they are compared with the results obtained from the full equations. In this section, the setup of the model to obtain the solution of the full set of equations in COMSOL Multiphysics® 5.6 is described. The system of Eqs. (24) and (27) is nonlinear and fully coupled. COMSOL is a commercial finite element package, and it uses the Galerkin finite element method to solve the system of partial differential equations (PDEs). The details of the model such as the flow geometries, meshes, boundary conditions, initial conditions, and solvers are described below.

For the Couette geometry, a rectangular domain is selected to be consistent with Fig. 2. The final domain is 1 unit long and 0.02 unit wide, with a quadrilateral mesh selected. The mesh independence study is conducted using the standard method by comparing the orientation profiles obtained for different mesh sizes. The final mesh consists of 16 000 elements with an average element quality of 1.0. For the slider bearing geometry, a domain in the shape of Fig. 3 is selected. A typical final mesh consists of 90 847 elements, with an average element quality of 0.7794. Mesh independency is confirmed by computing the orientation angle in the center of the domain as mesh refines. For both geometries investigated in this paper, COMSOL simulations are performed in two-dimensional (2D) domains.

For both the Couette flow geometry and the slider bearing geometry, initially, the flow field is set to be at rest, and the initial conditions of the \mathbf{Q} tensor are set to be a homogeneous orientation field with superposed infinitesimal fluctuations, as shown below [37]:

$$\mathbf{Q} = S_{\text{eq}}(\mathbf{nn} - \frac{1}{3}\mathbf{I}) ; \quad \mathbf{n} = (\cos(\varepsilon\xi), \sin(\varepsilon\xi), 0), \quad (42)$$

where $\varepsilon = \frac{\pi}{180} \times 10^{-4}$ and ξ is a Gaussian noise.

For the Couette geometry, the inlet and outlet are set to periodic boundary conditions. The top wall is set to be a sliding wall with the no-slip condition. The lower wall is stationary, and the no-slip condition is used. The boundary condition in the PDE module is set as periodic boundary conditions at the inlet and the outlet. The top wall and the lower wall are given Dirichlet boundary conditions, and the value is set to planar orientation. For the slider bearing geometry, in the flow module, the inlet and the outlet are set to be zero pressure. For the orientation, the top wall is stationary, and the no-slip condition is used. The lower wall is set to be a sliding wall with the no-slip condition and is driven by a velocity. In the PDE module, periodic boundary conditions are used for the inlet and the outlet. Dirichlet boundary conditions are given to the top wall and the lower wall with values set to planar orientation. The COMSOL codes for solving the full LdG equations have been validated in Refs. [5], [9], and [16].

The time stepping is performed using the backward differentiation formula (BDF) and the multifrontal massive parallel sparse direct solver (MUMPS) is used to invert the generated matrix. The tolerance of the solver is set as 10^{-8} and the solution is computed until a steady state is reached.

The simplified nondimensional evolution equations are shown in Eqs. (35)–(37). Similar to the solution procedure for the full equations, COMSOL Multiphysics® is used to solve Eqs. (35)–(37) coupled with Eq. (27) as momentum equations. The flow geometries, mesh sizes, boundary conditions, initial conditions, and solvers are virtually identical to those for the full equations except that the stationary solvers in COMSOL are used.

In the simulations of both the simplified equations and the full equations for both the Couette and the slider bearing geometries, the following parameter values are chosen: $\beta = 1$, $\mathfrak{A} = 4$, and $L^* = 0.45$ [16]. Landau viscosities are chosen as $\nu_1^* = 1$, $\nu_2^* = -1$, and $\nu_4^* = 6$ [16].

IV. RESULTS AND DISCUSSION

In this section, the simplified LdG model is first evaluated and verified by plotting the orientation profiles across the gap as Er increases until flow alignment in the Couette geometry. Then, the flow curve is plotted from both sets of equations solved over the Couette geometry. The flow in the Couette geometry is solved for $De = 1$ and $Re = 10^{-4}$. The nondimensional parameters are selected in accordance with [42]. It is important to note that the Re in this article is defined in a way

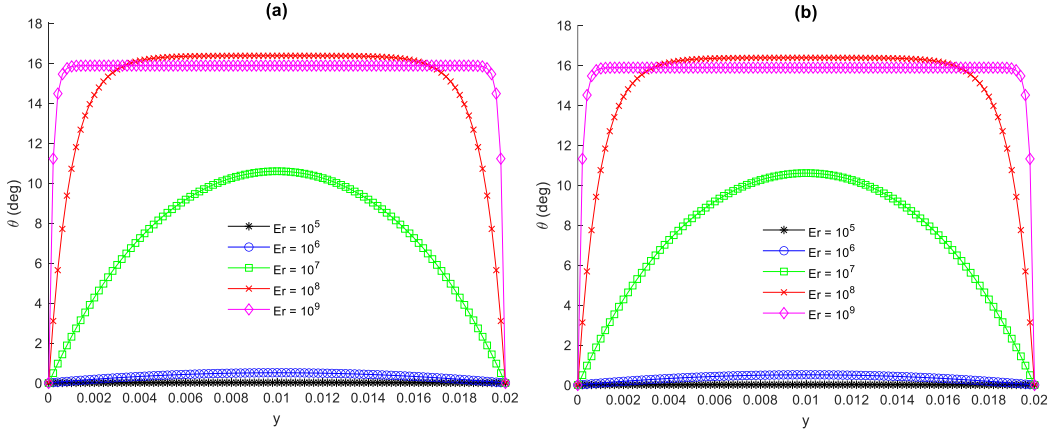


FIG. 4. Orientation profiles from (a) the simplified LdG equations, and (b) the full LdG equations.

different from the conventional Re , meaning that it is not appropriate to compare the value of the Re in this article with the those of the conventional Re .

Figures 4(a) and 4(b) show how the orientation profiles across the gap change in the Couette flow geometry as Er increases in the simplified LdG model and the full LdG model, respectively. Because the LC is flow aligning, under shear, the director of the LC is expected to make an angle with the flow direction, known as the flow-alignment angle. As Er increases, the orientation angles increase toward the flow-alignment angle, which is 16.62° , a material property computed as a function of S_{eq} and β [14]. The behavior of LCs under shear is determined by another material property parameter, namely the reactive parameter λ [10]. λ is computed as the ratio of the irrotational viscosity to the rotational torque coefficient. If the absolute value of λ is greater than 1, the LC is flow aligning, meaning that its director flow-aligns the shearing velocity, by an angle known as the flow alignment angle ($\theta_{al} = \frac{1}{2} \cos^{-1}(\frac{1}{\lambda})$). θ_{al} can also be computed as $\theta_{al} = \frac{1}{2} \cos^{-1}(\frac{6S}{\beta(4+2S-S^2)})$. Since the flow-alignment angle is a material property, reaching flow alignment under strong shear is a method to evaluate and verify the flow simulation of flow-aligning LCs [10]. When the absolute value of λ is between 0 and 1, flow alignment does not occur. λ of rodlike LCs is greater than 0 whereas λ of disklike LCs is smaller than 0 [10]. The good agreement between the theoretical and computational flow-alignment verifies the simplified LdG equations. Moreover, the good agreement between Figs. 4(a) and 4(b) at all Er further verifies the simplified LdG model.

Figures 5(a) and 5(b) show the scalar order parameter (S) profiles across the gap as a function of y in the simplified LdG model and the full LdG model, respectively. As both plots show, as Er increases, the value of S remains close to $S_{eq} = 0.683$, thus indicating that the flow is orientation-dominated, which means that the flow affects the eigenvectors of \mathbf{Q} but not the eigenvalues [14,43]. The small deviation of S from S_{eq} indicates a small degree of biaxiality but the flow is still predominantly uniaxial.

First, Fig. 6 shows that the dimensionless viscosities at various dimensionless shear rates computed from the simplified LdG model and the full LdG model are in very good agreement. Second, as the shear rate increases, the apparent viscosity also increases until a plateau is reached. The apparent shear-thickening behavior can be explained by the parallel boundary conditions of LCs and Miesowicz shear viscosities [14]: as the shear rate increases, the orientation angle measured with respect to the x axis also increases, which causes an increase in flow resistance, thus increasing the apparent viscosity; the Newtonian plateau is well documented in the flow curve of LCs [1].

For the slider bearing geometry, the dimensionless pressure and orientation profiles are plotted as the pitch angle increases; the dimensionless load-carrying capacity, the friction force, and the coefficient of friction (COF) are also computed at various pitch angles. The flow in the slider bearing

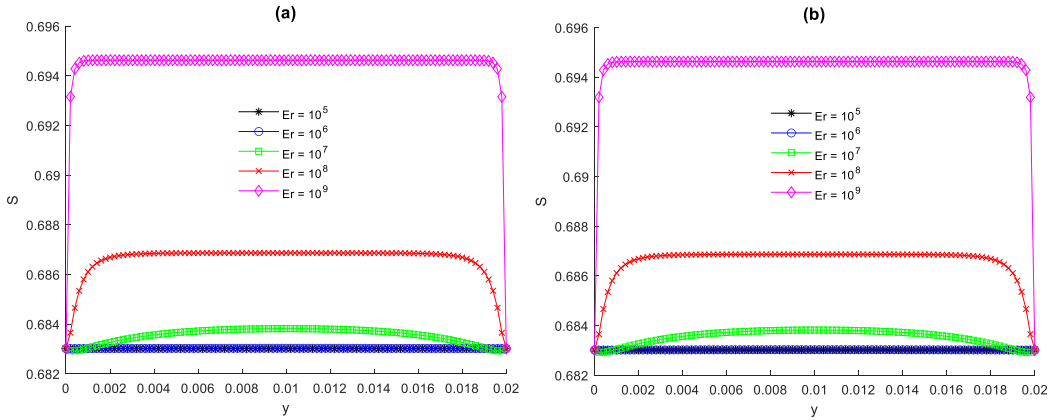


FIG. 5. Scalar order parameters from (a) the simplified LdG equations, and (b) the full LdG equations.

geometry is solved for $De = 1$, $Er = 10^6$, and $Re = 1$ [42]. A higher value of Re is selected for the LC flow in the slider bearing geometry than that in the Couette geometry for the purpose of increasing viscous effects expected in a slider bearing. Since the governing equations are dimensionless, all quantities and variables computed in this section, including pressure, load-carrying capacity, and friction force, are also dimensionless, except for the orientation angles.

Figures 7(a) and 7(b) show good agreement between the dimensionless pressure profiles from the full and the simplified LdG models in the slider bearing geometry, thus further verifying the simplified LdG model. The shape of the dimensionless pressure profiles is characteristic of flows in slider bearing geometries with both Newtonian fluids and non-Newtonian fluids [22,32] as lubricants. Although in this study, the LdG theory is used for modeling the flow of LCs, the pressure profiles obtained from the lubrication approximation of the LdG model are qualitatively similar to those obtained from the lubrication approximation of the EL theory [22], which again verifies the proposed simplified model. In those figures, as the pitch angle increases, so do the filmwise pressure profiles, which also indicates a higher load-carrying capacity. This result is consistent with slider

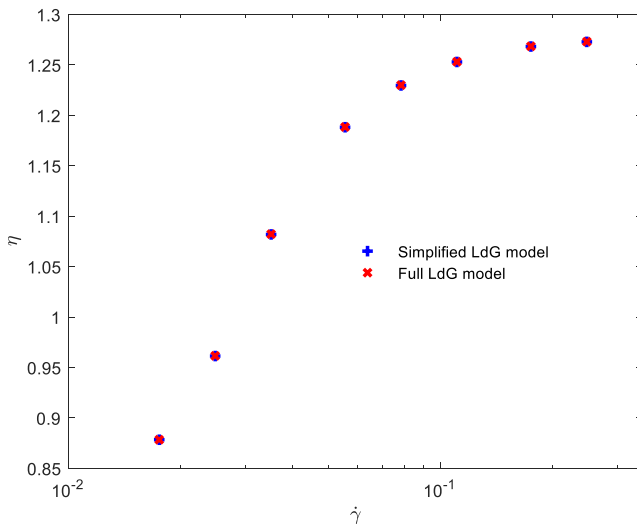


FIG. 6. Dimensionless viscosity at various dimensionless shear rates.

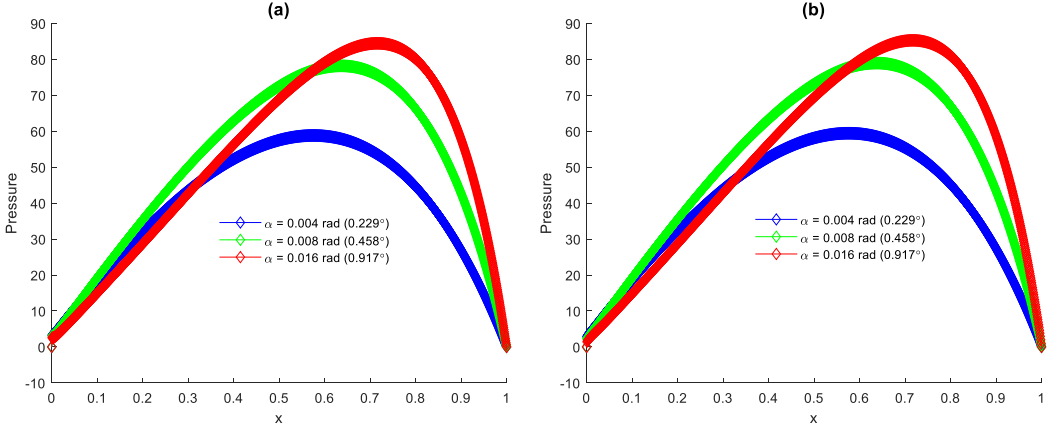


FIG. 7. Pressure profiles at various pitch angles from (a) the simplified LdG equations, and (b) the full LdG equations.

bearings with Newtonian fluids, which is established in the literature [44]. Figures 8(a), 8(b), 9(a), and 9(b) show that there is good agreement between the orientation profiles and the scalar order parameters from the full and the simplified LdG models, which further verifies the simplified LdG model. The flow-alignment angle, in this case, is again 16.62° , because similar parameters are used to solve the flow in the slider bearing geometry. As Figs. 9(a) and 9(b) show, the value of S is slightly larger than $S_{eq} = 0.683$, but S is still close to S_{eq} , indicating a small deviation from uniaxiality, though the deviation is larger in this case than that in the Couette flow geometry.

As presented in Tables I–III, the dimensionless load-carrying capacity (F_{load}), friction force (F_{fric}) and COF at various pitch angles in the slider bearing geometry for both the simplified LdG model and the full LdG model in COMSOL Multiphysics® are computed. Their expressions are shown below [22]:

$$F_{load} = - \int_0^L (-p + \sigma_{yy}) dx = \int_0^L (p - \sigma_{yy}) dx, \quad (43)$$

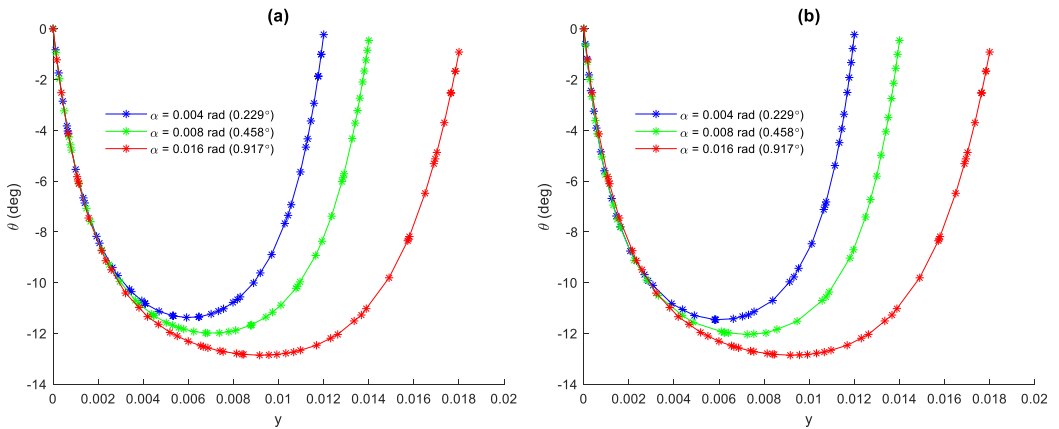


FIG. 8. Orientation profiles at various pitch angles from (a) the simplified LdG equations, and (b) the full LdG equations.

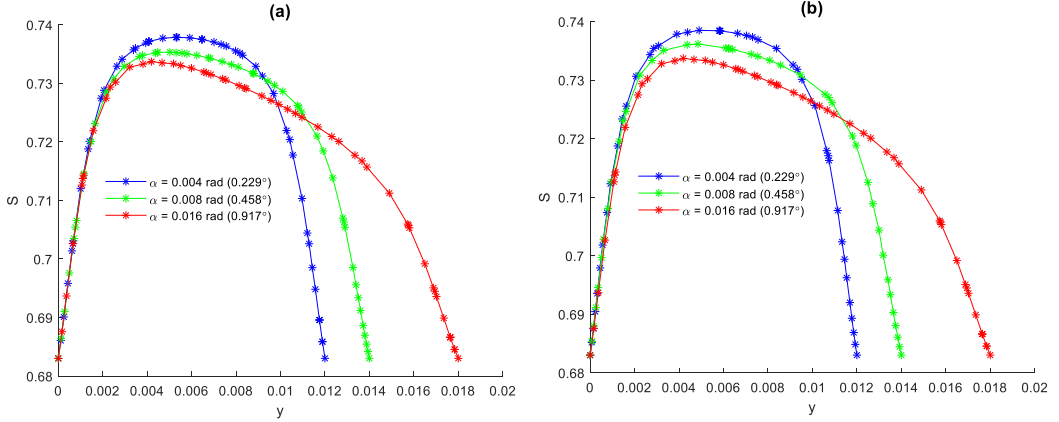


FIG. 9. Scalar order parameters from (a) the simplified LdG equations, and (b) the full LdG equations.

$$F_{\text{fric}} = - \int_0^L (\sigma_{xy}) dx, \quad (44)$$

$$\text{COF} = \frac{F_{\text{fric}}}{F_{\text{load}}}, \quad (45)$$

where all variables are dimensionless with the asterisk dropped for simplicity. The integrations are performed in COMSOL with the line integration function along the lower plate of the slider bearing with L being the length of the slider bearing. In Eq. (43), p is the dimensionless pressure and σ_{yy} is the yy component of the dimensionless total stress tensor both evaluated at the lower plate. In Eq. (44), σ_{xy} is the xy component of the dimensionless total stress tensor evaluated at the lower plate.

In Tables I–III, the simplified LdG model and the full LdG model also produce similar results in load-carrying capacity, friction force, and COF, as demonstrated by the small percent errors among all quantities. As shown in Table I, as the pitch angle increases, so does the load-carrying capacity, which is consistent with Figs. 7(a) and 7(b). Table II shows that as the pitch angle increases, the friction reduces; Table III indicates that as the pitch angle increases, the COF decreases. These results are consistent with slider bearings with Newtonian fluids as lubricants [44] as well as those with power-law fluids as lubricants [45]. The values of the COF as shown in Table III are consistent with the results from other studies regarding LCs [46,47].

As expected, the simplified LdG model takes much less time to solve than the full LdG model in COMSOL. On average, it takes around 2 h to solve the full LdG model but only 2 min to solve the corresponding simplified LdG model over the same mesh sizes, which amounts to a 98.3% reduction in simulation wall time, with both models solved on a workstation equipped with an Intel® Core i7-6700 CPU (four cores with eight processors and 16 GB of total RAM). The drastic reduction in wall time not only allows rapid prototyping in model building, but saves computational resources, which are both advantages of the simplified LdG model over the full LdG model.

TABLE I. Dimensionless load-carrying capacity at various pitch angles.

Pitch angle (α)	Simplified LdG model	Full LdG model	% error
0.004 rad (0.229°)	42.30	42.74	1.03
0.008 rad (0.458°)	53.73	54.23	0.92
0.016 rad (0.917°)	54.63	55.08	0.82

TABLE II. Dimensionless friction force at various pitch angles.

Pitch angle (α)	Simplified LdG model	Full LdG model	% error
0.004 rad (0.229 °)	2.86	2.89	0.89
0.008 rad (0.458 °)	2.66	2.69	0.84
0.016 rad (0.917 °)	2.49	2.51	0.89

V. CONCLUSION

The LdG equations modeling the flow of LCs are simplified using the Reynolds scaling analysis (lubrication theory) to reduce the required computational resources. The proposed simplified LdG model is applied to the Couette flow geometry and the slider bearing geometry. Then, the simplified LdG model is evaluated and verified by comparing the alignment angle with its theoretical value in the Couette flow geometry. A flow curve of LCs consistent with the literature is also obtained. For the slider bearing geometry, an increase in pitch angles corresponds to a rise in filmwise pressure, thus improving the load-carrying capacity and reducing the COF. The computed COFs also agree with the literature value of LC lubricants. The good agreement between the results obtained using the simplified LdG model and the full LdG model with small percent errors further verifies the simplified LdG model. The large reduction in wall time (98.3%) as a result of applying the simplified LdG model significantly reduces the computational resource needed to perform the simulations.

This study simplifies the LdG model using the Reynolds scaling analysis. The results of the parametric studies from the simplified LdG model are particularly helpful for the design of bearings in the industry, where engineers and scientists can perform parametric studies to determine a set of design parameters that maximize the load-carrying capacity and minimize the COF. The simplified LdG model can be applied to other 2D thin-gap geometries, such as that of a journal bearing. The use of the simplified LdG equations results in a large decrease in wall time, which has the potential to significantly reduce the computational resources needed for simulating LC flows in complex geometries, which can save time, energy, and resources.

One limitation of this research is that only defect-free cases are investigated. To simulate defects in LCs, more complex flow geometries such as that of a journal bearing can be studied. As for future work, since many complex flow geometries are 3D, it may be beneficial to extend the equations to 3D flows. Also, although our previous work is focused on computation, it may be possible to express the solution to the lubrication approximation analytically as an integral solution.

ACKNOWLEDGMENTS

D.G. acknowledges financial support from the Natural Sciences and Engineering Research Council of Canada (NSERC) Discovery Grant. S.L. acknowledges financial support from the UBC Gartshore Scholarship. S.B. acknowledges the MITACS Globalink Graduate Fellowship for financial support. The authors gratefully acknowledge WestGrid and the Digital Research Alliance of Canada for providing computational resources for this research.

TABLE III. COF at various pitch angles.

Pitch angle (α)	Simplified LdG model	Full LdG model	% error
0.004 rad (0.229 °)	0.0677	0.0676	0.15
0.008 rad (0.458 °)	0.0496	0.0496	0.10
0.016 rad (0.917 °)	0.0456	0.0457	0.09

- [1] R. G. Larson, *The Structure and Rheology of Complex Fluids* (Oxford University Press, New York, 1999).
- [2] B. Bhushan, *Introduction to Tribology* (John Wiley & Sons Inc., Hoboken, 2013).
- [3] Z. M. Jin and D. Dowson, A full numerical analysis of hydrodynamic lubrication in artificial hip joint replacements constructed from hard materials, *Proc. Inst. Mech. Eng., Part C* **213**, 355 (1999).
- [4] M. Shariatzadeh and D. Grecov, Aqueous suspensions of cellulose nanocrystals as water-based lubricants, *Cellulose* **26**, 4665 (2019).
- [5] N. Noroozi and D. Grecov, Flow modelling and rheological characterization of nematic liquid crystals between concentric cylinders, *Liq. Cryst.* **40**, 871 (2013).
- [6] F.-J. Carrión, G. Martínez-Nicolás, P. Iglesias, J. Sanes, and M.-D. Bermúdez, Liquid crystals in tribology, *Int. J. Mol. Sci.* **10**, 4102 (2009).
- [7] B. I. Kupchinov, V. G. Rodnenkov, S. F. Ermakov, and V. P. Parkalov, A study of lubrication by liquid crystals, *Tribol. Int.* **24**, 25 (1991).
- [8] H. A. Elemsimit and D. Grecov, Impact of liquid crystal additives on a canola oil-based bio-lubricant, *Proc. Inst. Mech. Eng., Part J* **229**, 126 (2015).
- [9] N. Noroozi and D. Grecov, Numerical simulation of three-dimensional flow-induced microstructure in a simplified prosthetic hip joint with nematic liquid crystal lubricant, *Rheol. Acta* **53**, 457 (2014).
- [10] G. P. G. de and J. Prost, *The Physics of Liquid Crystals* (Oxford University Press, Oxford, 1995).
- [11] Y. Farhodi and A. D. Rey, Shear flows of nematic polymers. I. Orienting modes, bifurcations, and steady state rheological predictions, *J. Rheol.* **37**, 289 (1993).
- [12] A. P. Singh and A. D. Rey, Microstructure constitutive equation for discotic nematic liquid crystalline materials. Part II. Microstructure-rheology relations, *Rheol. Acta* **37**, 374 (1998).
- [13] T. Tsuji and A. D. Rey, Effect of long range order on sheared liquid crystalline materials: Part 1: Compatibility between tumbling behavior and fixed anchoring, *J. Non-Newtonian Fluid Mech.* **73**, 127 (1997).
- [14] D. Grecov and A. D. Rey, Theoretical and computational rheology for discotic nematic liquid crystals, *Mol. Cryst. Liq. Cryst.* **391**, 57 (2002).
- [15] A. P. Singh and A. D. Rey, Effect of long-range elasticity and boundary conditions on microstructural response of sheared discotic mesophases, *J. Non-Newtonian Fluid Mech.* **94**, 87 (2000).
- [16] N. Noroozi and D. Grecov, Numerical simulation of flow and structure in nematic liquid crystalline materials between eccentric cylinders, *J. Non-Newtonian Fluid Mech.* **208–209**, 1 (2014).
- [17] A. N. Beris and B. J. Edwards, *Thermodynamics of Flowing Systems: With Internal Microstructure* (Oxford University Press, New York, 1994).
- [18] T. Qian and P. Sheng, Generalized hydrodynamic equations for nematic liquid crystals, *Phys. Rev. E* **58**, 7475 (1998).
- [19] O. Reynolds, IV. On the theory of lubrication and its application to Mr. Beauchamp tower's experiments, including an experimental determination of the viscosity of olive oil, *Philos. Trans. R. Soc. London* **177**, 157 (1886).
- [20] L. G. Leal, *Advanced Transport Phenomena: Fluid Mechanics and Convective Transport Processes* (Cambridge University Press, Cambridge, UK, 2010).
- [21] J. A. Tichy, Hydrodynamic lubrication theory for the Bingham plastic flow model, *J. Rheol.* **35**, 477 (1991).
- [22] J. A. Tichy, Lubrication theory for nematic liquid crystals, *Tribol. Trans.* **33**, 363 (1990).
- [23] V. N. Constantinescu, On turbulent lubrication, *Proc. Inst. Mech. Eng.* **173**, 881 (1959).
- [24] N. Naduvinamani and G. Marali, Dynamic Reynolds equation for micropolar fluid lubrication of porous slider bearings, *J. Mar. Sci. Technol.* **16**, 182 (2008).
- [25] S. A. Roberts, D. R. Noble, P. R. Schunk, and E. M. Benner, Multiphase hydrodynamic lubrication flow using a three-dimensional shell finite element method, *Comput. Fluids* **87**, 12 (2013).
- [26] S. Takeuchi and J. Gu, Extended Reynolds lubrication model for incompressible Newtonian fluid, *Phys. Rev. Fluids* **4**, 114101 (2019).
- [27] M. Ben Amar and L. J. Cummings, Fingering instabilities in driven thin nematic films, *Phys. Fluids* **13**, 1160 (2001).

- [28] L. J. Cummings, Evolution of a thin film of nematic liquid crystal with anisotropic surface energy, *Eur. J. Appl. Math.* **15**, 651 (2004).
- [29] B. Y. Ballal and R. S. Rivlin, Flow of a Newtonian fluid between eccentric rotating cylinders: Inertial effects, *Arch. Ration. Mech. Anal.* **62**, 237 (1976).
- [30] X. K. Li, Non-Newtonian lubrication with the Phan-Thien–Tanner model, *J. Eng. Math.* **87**, 1 (2014).
- [31] D. Grecov and J.-R. Clermont, Numerical simulations of non-Newtonian flows between eccentric cylinders by domain decomposition and stream-tube method, *J. Non-Newtonian Fluid Mech.* **126**, 175 (2005).
- [32] C. Dorier and J. Tichy, Behavior of a bingham-like viscous fluid in lubrication flows, *J. Non-Newtonian Fluid Mech.* **45**, 291 ((1992)).
- [33] R. H. Buckholz, Effects of power—law, non-Newtonian lubricants on load capacity and friction for plane slider bearings, *J. Tribol.* **108**, 86 (1986).
- [34] L.-M. Chu, H.-C. Hsu, and J.-L. Chen, An analytical approach for analysis of bearings with non-Newtonian lubricants, *Adv. Mech. Eng.* **6**, 404759 (2014).
- [35] B. I. Kupchinov, S. F. Ermakov, V. G. Rodnenkov, S. N. Bobrysheva, and E. D. Beloenko, The effect of liquid crystals on joint lubrication, *Wear* **171**, 7 (1994).
- [36] N. M. Bujurke, Slider bearings lubricated by a second-grade fluid with reference to synovial joints, *Wear* **78**, 355 (1982).
- [37] A. D. Rey and T. Tsuji, Recent advances in theoretical liquid crystal rheology, *Macromol. Theory Simul.* **7**, 623 (1998).
- [38] D. Grecov and A. D. Rey, Transient rheology of discotic mesophases, *Rheol. Acta* **42**, 590 (2003).
- [39] D. Grecov and A. D. Rey, Shear-induced textural transitions in flow-aligning liquid crystal polymers, *Phys. Rev. E* **68**, 061704 (2003).
- [40] R. L. Panton, *Incompressible Flow* (John Wiley & Sons, Hoboken, 2013).
- [41] M. W. Johnson and S. Mangkoesobroto, Analysis of lubrication theory for the power law fluid, *J. Tribol.* **115**, 71 (1993).
- [42] A. D. Rey, Liquid crystal models of biological materials and processes, *Soft Matter* **6**, 3402 (2010).
- [43] A. D. Rey and E. E. Herrera-Valencia, 7 - Theory and simulation of flow-induced microstructures in liquid crystalline materials, in *Flow-Induced Alignment in Composite Materials*, 2nd ed. (Woodhead, Duxford, 2022), pp. 229–277.
- [44] A. W. Batchelor and G. W. S. Stachowiak, Chapter 4 - Hydrodynamic lubrication, in *Engineering Tribology* (Butterworth-Heinemann, Amsterdam, 2014), pp. 105–210.
- [45] N. C. Das, A study of optimum load capacity of slider bearings lubricated with power law fluids, *Tribol. Int.* **32**, 435 (1999).
- [46] S. Mori and H. Iwata, Relationship between tribological performance of liquid crystals and their molecular structure, *Tribol. Int.* **29**, 35 (1996).
- [47] Z. Li, C. Xu, G. Xiao, J. Zhang, Z. Chen, and M. Yi, Lubrication performance of graphene as lubricant additive in 4-n-pentyl-4'-cyanobiphenyl liquid crystal (5CB) for steel/steel contacts, *Materials (Basel)* **11**, 2110 (2018).